JOURNAL OF SPACECRAFT AND ROCKETS
Vol. 46, No. 4, July–August 2009

Above the Horizon Satellite Coverage with Dual-Altitude Band Constraints

Belinda G. Marchand*
University of Texas at Austin, Austin, Texas 78712
and
Christopher J. Kobel
The Aerospace Corporation, El Segundo, California 90009

DOI: 10.2514/1.37140

The optimal satellite coverage problem traditionally refers to maximizing the visibility of targets against an Earth background. In this study, the focus shifts to satellite coverage of targets against a space background within a dual-altitude band defined by an upper and a lower target altitude. Furthermore, because objects against an Earth background are outside the region of interest, the coverage area to be maximized exists above the local horizon and, naturally, within a prespecified sensor range. The present analysis is restricted to satellites on circular orbits to simplify the mathematical development of the objective function. In the course of this development, geometrical arguments are employed to identify an analytical expression for the resulting coverage area. A graphical analysis tool, developed during the course of this study, is employed to develop new insight into how the coverage area is affected by changes in the mutual intersection of these reference surfaces. The result of the study is an objective function that can be employed in an optimization process in the search for optimal satellite constellations that maximize coverage of the area of interest.

Nomenclature

$\mathbf{A}(\cdot)$	=	area operator
$\tilde{\mathbf{A}}(\cdot)$	=	complement of the area operator
$\mathbf{A}_{\mathrm{RS}\cap\mathrm{LTAS}}$	=	area of intersection within the range shell and the lower target altitude shell
$\mathbf{A}_{\mathrm{RS}\cap\mathrm{UTAS}}$	=	area of intersection within the range shell and the upper target altitude shell
$\mathbf{A}_{\triangle}(\cdot)$	=	area of a triangle
$\mathbf{A}_{\Lambda_i}(\cdot)$	=	area of a type i composite triangle, for $i = 1$ or 2
$\mathbf{A}_{\pi_1}(\cdot)$	=	area of a circular sector
$\mathbf{A}_{\pi_2}(\cdot)$	=	area of a teardrop sector
$\mathbf{A}_{\Sigma}(\cdot)$	=	area of a circular segment
R	=	radius of the range shell
R_e	=	radius of the Earth
r_l	=	radius of the lower target altitude shell
r_s	=	radial distance from center of the planet to the satellite
r_t	=	radius of the tangent height shell
r_{tar}	=	target radius of altitude shell used in the traditional single band above the horizon coverage problem
r_u	=	radius of the upper target altitude shell
$\hat{x}$	=	$\hat{y} \times \hat{z}$
(x, y)	=	with the appropriate subscript, denotes Cartesian coordinates of a point
$\hat{y}$	=	unit vector directed from the center of the Earth to the satellite
$\hat{z}$	=	unit vector normal to the plane of motion of the satellite, along the angular momentum vector
θ	=	below the horizon coverage angle
θ_{in}	=	above the horizon entry coverage angle
θ_{out}	=	above the horizon exit coverage angle
θ_t	=	above the horizon coverage angle at the tangent point

Subscripts

A	=	intersection between a target shell and the tangent line that is farthest from r_s
B	=	intersection between a target shell and the tangent line that is closest to r_s
S	=	quantity associated with the satellite
$\triangle$	=	quantity associated with a triangle
Λ_1	=	quantity associated with a type 1 composite triangle
Λ_2	=	quantity associated with a type 2 composite triangle
Σ	=	quantity associated with a circular segment
1	=	intersections to the right of r_s
2	=	intersections to the left of r_s

Superscripts

$\overset{\frown}{\ }$	=	circular segment
$\overline{\ }$	=	line segment
$\overline{\lvert\ \rvert}$	=	magnitude of a line segment

I. Introduction

THE available literature on satellite and constellation coverage typically focuses on sensor visibility against an Earth background [1]. For example, constellations designed for continuous global coverage [1–6] can be qualified under the purview of below the horizon (BTH) coverage [7], sometimes termed as coverage below the tangent height. The horizon, in this case, is not necessarily defined relative to the Earth's limb. Instead, it may be defined relative to the closest distance to the Earth's limb where objects are still visible to the onboard sensors. This minimum distance is referred to as the tangent height [7], a characteristic specific to the sensor under consideration. In this study, it is advantageous to define a related reference surface, the tangent height shell (THS). The THS is a sphere, concentric with the Earth, for which the radius exceeds that of the Earth's by the tangent height. An imaginary tangent line (TL), originating from the satellite and tangent to any point on the surface

Presented at the AAS/AIAA Space Flight Mechanics Winter Meeting Paper AAS 08-247, The San Luis Resort, Galveston, TX, 27–31 January 2008; received 14 February 2008; accepted for publication 24 November 2008. Copyright © 2009 by The Aerospace Corporation. Published by the American Institute of Aeronautics and Astronautics, Inc., with permission. Copies of this paper may be made for personal or internal use, on condition that the copier pay the $10.00 per-copy fee to the Copyright Clearance Center, Inc., 222 Rosewood Drive, Danvers, MA 01923; include the code 0022-4650/09 $10.00 in correspondence with the CCC.

*Member AIAA.

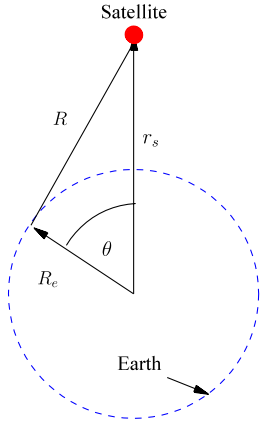

Fig. 1 BTH coverage geometry.

of the THS, traces a conical shape defined here as the tangent height cone (THC). Consistent with this terminology, the region of interest in BTH coverage corresponds to the region inside the THC. Thus, BTH coverage refers to more than just ground coverage; it also encompasses coverage of everything the sensors can see below the horizon, ground-based or otherwise. In general, the literature on constellations for global coverage is quite extensive. However, to offer a representative sample, earlier studies by Walker [2–4], Adams and Rider [5], and Lang [6] can all, in a sense, be qualified as a subset of BTH coverage, even if not always explicitly stated.

Maximizing BTH coverage [8–11] refers to the identification of constellation and satellite orbital parameters that maximize the entire area visible to the sensors below the horizon. For a single satellite, the altitude that leads to maximum BTH coverage depends on the capabilities of the sensor. The computation is straightforward if the satellite is assumed to evolve along a circular orbit and the sensor range can be modeled as omnidirectional. For instance, in Fig. 1, the BTH area covered by a single satellite evolving along a circular orbit is maximized when θ is maximized for a given R. That is, the maximum θ occurs when the satellite altitude is such that R and R_e form a right triangle, which leads to $\theta = \tan^{-1}(R/R_e)$.

In constellation design, the optimal BTH coverage problem seeks to identify the minimum number of satellites required to achieve continuous coverage and maximize the visible area below the horizon. A similar goal is applicable in designing constellations that guarantee continuous coverage above the horizon (ATH) with a minimum number of satellites [8–11]. Earlier studies on ATH coverage [8–11] focus on optimal constellations for single-altitude band ATH coverage. This refers to maximizing the sensor visibility above the horizon and within a single prespecified target altitude. For example, the illustration in Fig. 2 presents a cross-sectional view of the Earth, the THS, and the target altitude shell. The line that originates at the satellite and is tangent to the THS at r_t is the TL. The TL crosses the target altitude shell at two different locations in this example. The first crossing occurs nearest to the satellite, a distance $R_2 - R_1$ from the vehicle. The second crossing takes place a distance $R_2 + R_1$ away from the satellite. The quantities R_1 and R_2 are e asily determined by direct application of the law of cosines and Pythagoras's theorem. Thus, R_1 and R_2 are functions of the problem parameters, r_s, r_t, and r_{tar}. The quantity $R_2 - R_1$ is useful in identifying the minimum sensor range required for ATH coverage at the specified altitude. Similarly, $R_2 + R_1$ defines the maximum value of the sensor range needed to cover everything inside the region

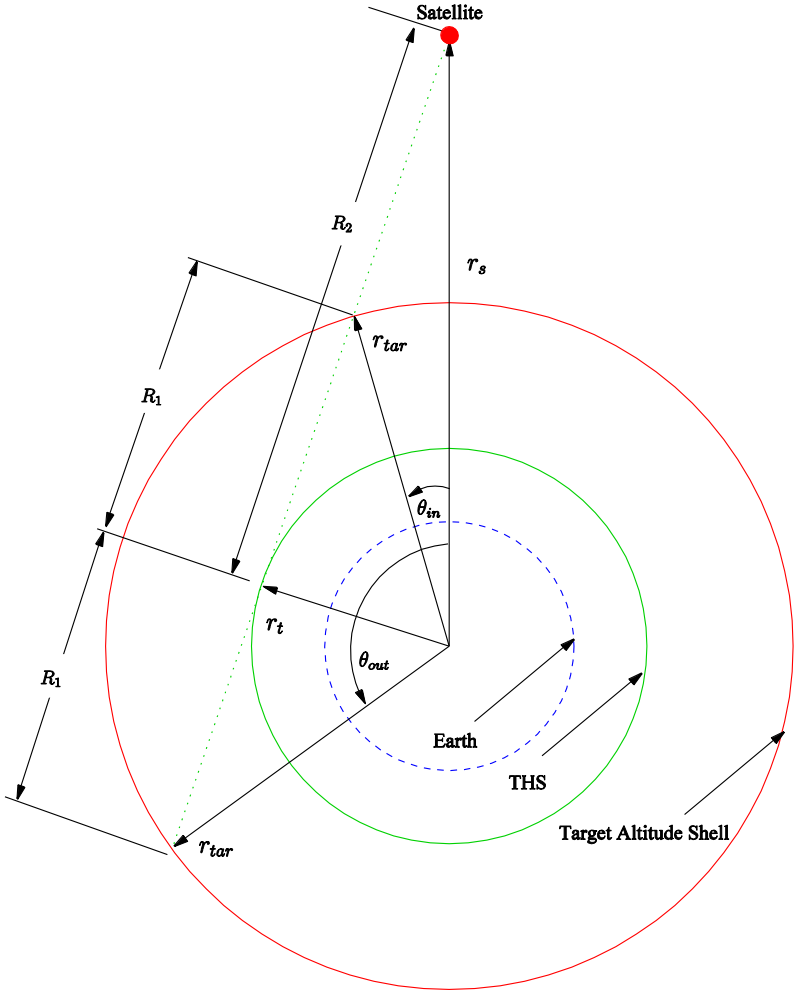

Fig. 2 Single-altitude band ATH coverage geometry.

bounded by the target altitude shell and the horizon. The variation in coverage area corresponding to these two limiting cases is illustrated by the shaded regions in Fig. 3.

It is apparent from Fig. 3 that there exists an altitude where sensor ranges greater than $R_2 + R_1$ do not offer any additional coverage of the target altitude band defined in Fig. 2. Given this information, maximizing ATH coverage within a single-altitude band requires that the satellite altitude be selected such that the sensor range equals $R_1 + R_2$. In that case, the coverage area is easily determined as the area of the circular segment in Fig. 2 with chord length $2R_1$. Of course, in Fig. 2, another region of coverage exists, one mirrored about the axis directed from the center of the Earth to the spacecraft. Because the sensor is omnidirectional, these two mirror sections ultimately represent the cross section of a three-dimensional coverage volume. The coverage volume is fixed and axially symmetric for a given satellite altitude. Therefore, maximizing the coverage volume is equivalent to maximizing the area of any cross section of that volume about any plane that contains the symmetry axis. As such, all figures presented in this study, specifically those that depict the satellite and the coverage area, are ultimately illustrative of the cross section of the coverage volume onto the satellite orbital plane.

Unlike single-altitude band ATH coverage [8–11], the present investigation focuses on dual-altitude band ATH coverage. This type of coverage refers to the visibility of objects that orbit within, or cross through, a region above the THC that exists within a prespecified altitude range. This range, termed the dual-altitude band, is characterized by a lower target altitude and an upper target altitude. The tangent height, and these target altitudes, are used to define three reference spheres concentric with the Earth. The THS is the smallest of these reference spheres. The lower target altitude shell (LTAS) is a reference spherical surface characterized by $r_l > r_t$, whereas the upper target altitude shell (UTAS) is associated with $r_u > r_l > r_t$. This initial work focuses strictly on identifying an analytical expression for the optimal single satellite altitude that maximizes dual-altitude band ATH coverage due to the complex coverage geometry.

The sensor is once again modeled as omnidirectional. Thus, the region visible to the satellite can be represented as a sphere, of radius R, centered at the satellite. This sphere is defined here as the range shell (RS). The RS moves with the satellite as it orbits the Earth. Assuming the satellite evolves along a circular orbit, the present study establishes a functional relation between the satellite altitude and the effective dual-altitude band ATH coverage area. That is, the area of the RS that exists below the UTAS, above the LTAS, and outside the THC. The result is a closed-form objective function that may be employed in any numerical optimization algorithm used in the design of constellations primarily aimed at providing maximum ATH coverage. Naturally, the objective function is only valid for satellites in circular orbits as that is a fundamental assumption at the present stage. Although generalizing these results to include elliptical orbits is desirable, it is outside the scope of the present study. Furthermore, it is important to note that maximizing coverage within a dual-altitude band may only represent one goal of a constellation. It may also be desirable to consider a multi-objective optimization where the goal is to maximize coverage within both a dual-altitude band and a latitude band. However, that application still benefits from knowledge of a closed-form equation that defines dual-altitude band ATH coverage as a function of satellite altitude, which is the only element considered in this investigation.

The determination of coverage area in the single-altitude band ATH coverage case is straightforward. In contrast, if r_t, r_u, r_l, and R are prespecified, identifying a functional relation between the dual-altitude band ATH coverage area and these parameters is not a straightforward process. However, a continuous piecewise differentiable function is ultimately identified here that successfully relates the dual-altitude band ATH coverage area to the satellite altitude, the tangent height, the upper target altitude, the lower target altitude, and the sensor range. The resulting objective function is then employed to identify the optimal altitude, for a single satellite, that maximizes coverage over a range of parameters.

Although there are undoubtedly multiple ways of formulating the associated objective function, the approach presented here is geometrical in nature [12]. Furthermore, the optimization process employed in the examples is a simple combination of grid and line search methods. The term grid search, as used here, implies the coverage area function is evaluated at a discrete set of evenly distributed satellite altitudes, upper target altitudes, lower target altitudes, and sensor ranges. From this grid, the maximum area, associated with a given set of parameters, is identified through programming logic and grid refinement. This is acceptable in this case because the study considers only one satellite. However, applying this objective function in a more complex constellation design problem would certainly benefit from a more sophisticated optimization approach. It is also important to note that, because the coverage area is a highly nonlinear function, a significant number of data points are required to capture the salient changes in area with altitude in the combined grid/line search method. The results of this analysis offer great insight into the evolution of the coverage area as a function of these parameters and constraints. The insight gained from

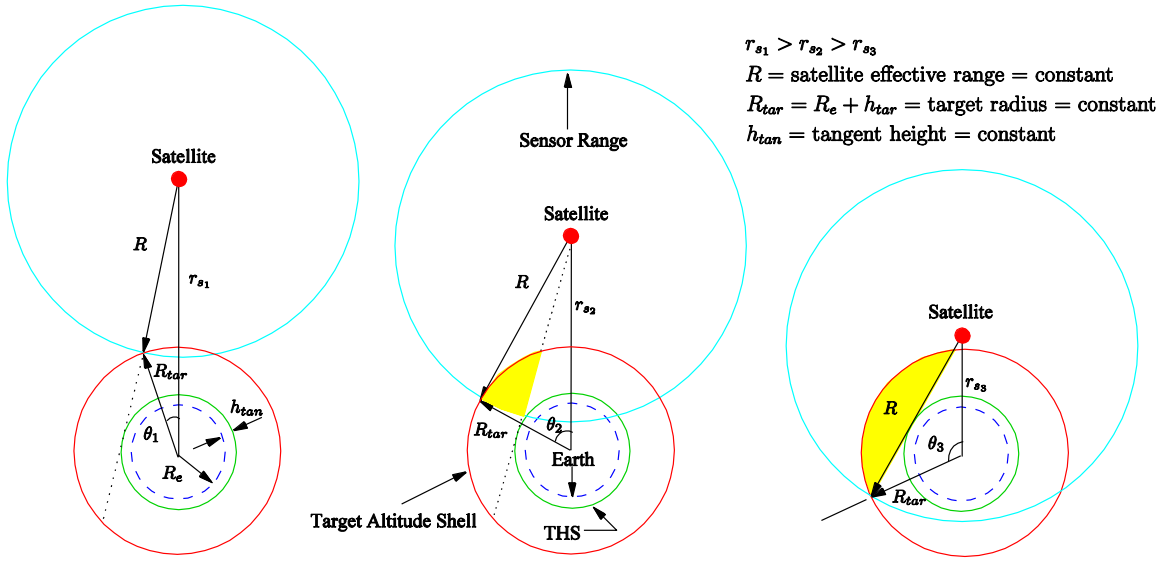

a) No ATH coverage **b) Some ATH coverage** **c) Maximum ATH coverage**

Fig. 3 ATH coverage changes with decreasing satellite altitude.

these results serves as a stepping stone to the more complex problem of constellation design.

II. Minimum Altitude and Condition for Zero Dual-Altitude Band Coverage Above the Horizon

In defining the range of altitudes to consider during a parametric study, it is advantageous to identify the minimum allowable satellite altitude and the altitude at which the satellite provides no ATH coverage. In this study, the minimum allowable altitude is defined as the tangent height. For example, if the THS defines the bounds of the atmosphere, and the sensors are unable to function properly in the presence of atmospheric interference, then the satellite cannot be placed below the THS. In contrast, the maximum altitude of interest corresponds to a point where $r_s > r_u$. As illustrated in Fig. 4, the satellite range offers no ATH coverage at a critical altitude r_{s_3}, given by

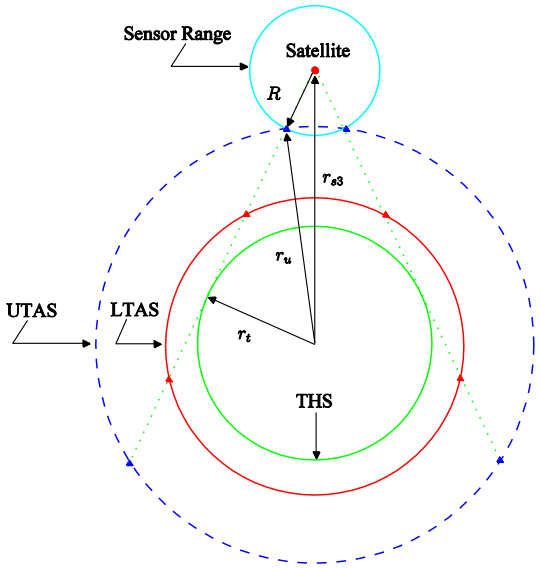

Fig. 4 Critical altitude for zero dual-altitude band ATH coverage, $r_s > r_u$.

$$r_{s_3} = \sqrt{(R + \sqrt{r_u^2 - r_t^2})^2 + r_t^2} \tag{1}$$

III. Shell Intersections

The geometry of coverage depends on a number of key intersections defined by the problem parameters: r_s, r_u, r_l, r_t, and R. In the algorithm presented here, the calculation of the coverage area is a function of the location of these key intersections. The results of this study reveal that no single closed-form equation exists to define the dual-altitude band ATH coverage area. At best, a continuous piecewise differentiable function may be defined. Also, in using the geometrical approach presented here, the representation of the coverage area is not unique because there are multiple ways of decomposing the coverage geometry into fundamental components. Figure 5 illustrates a sample geometry that depicts all possible intersection scenarios between the RS, TL, LTAS, and UTAS. This illustration is useful in establishing the basic notation employed in this study. It is evident that the maximum number of intersections possible is 14. Out of this maximum number of intersections, the only ones guaranteed to exist for all parameters are (T_1, T_2), (L_{1A}, L_{2A}), and (U_{1A}, U_{2A}). The remaining intersections may or may not exist

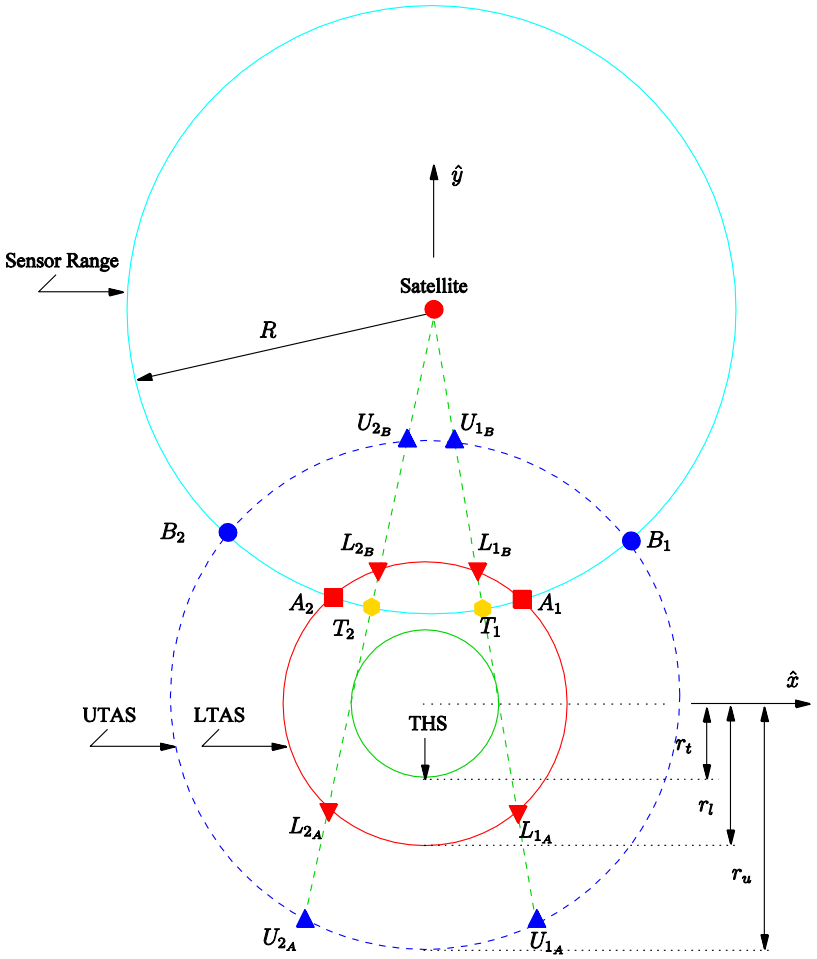

Fig. 5 Shell intersections.

depending on the satellite altitude and the size of the RS. For example, (U_{1B}, U_{2B}) exist only if the satellite is above the UTAS. Similarly, (L_{1B}, L_{2B}) exist only if the satellite is above the LTAS. Also, (A_1, A_2) and (B_1, B_2) exist if the RS intersects the LTAS and UTAS, respectively.

To simplify the process of ultimately extending the present results to satellite constellations, a rotating coordinate system is selected and all intersections are determined relative to this coordinate system. In this frame, the rotating $\hat{y}$ axis is the line from the center of the Earth to the satellite, and the $\hat{x}$ axis is in the plane of the orbit of the satellite and perpendicular to the $\hat{y}$ axis, as illustrated in Fig. 5. As such, the location of the satellite in this rotating coordinate frame is always given by $(x_s, y_s) = (0, r_s)$.

A. Intersections of the Range Shell with the Upper and Lower Target Altitude Shells

The intersection of the RS with the UTAS (B_1, B_2) is easily computed by simultaneously solving the mathematical relations that define the UTAS and the RS. At the point where the RS and UTAS intersect, the following pair of equations must be satisfied:

$$x_{B_1}^2 + (y_{B_1} - r_s)^2 = R^2; \qquad x_{B_1}^2 + y_{B_1}^2 = r_u^2 \tag{2}$$

The solution to this system of equations is given by

$$y_{B_1} = \frac{(r_u^2 + r_s^2 - R^2)}{2r_s}; \qquad x_{B_1} = \sqrt{r_u^2 - y_{B_1}^2} \tag{3}$$

Of course, the symmetrical nature of the arrangement further implies that

$$x_{B_2} = -x_{B_1}; \qquad y_{B_2} = y_{B_1} \tag{4}$$

A similar result applies for intersections at A_1 and A_2,

$$y_{A_1} = \frac{(r_l^2 + r_s^2 - R^2)}{2r_s}; \qquad x_{A_1} = \sqrt{r_l^2 - y_{A_1}^2} \tag{5}$$

$$x_{A_2} = -x_{A_1}; \qquad y_{A_2} = y_{A_1} \tag{6}$$

B. Intersections of the Tangent Line with the Lower Target Altitude Shell

The TL originates at the satellite (x_s, y_s) and extends down toward the THS such that the intersection is tangent when

$$\theta_t = \cos^{-1}\left(\frac{r_t}{r_s}\right) \tag{7}$$

as illustrated in Fig. 5. Based on this definition, the slope of the TL may be expressed in terms of the position of the satellite and the coordinates of the intersection as follows:

$$m = \frac{y_t - y_s}{x_t - x_s} \tag{8}$$

for $x_t = \pm r_t \sin\theta_t$ and $y_t = r_t \cos\theta_t$.

Let $(x_{L_{1A/B}}, y_{L_{1A/B}})$ denote the Cartesian coordinates of L_{1A} or L_{1B}. Then, the intersection of the LTAS with the TL is given by the solution to the following system of equations:

$$x_{L_{1A/B}}^2 + y_{L_{1A/B}}^2 = r_l^2; \qquad y_{L_{1A/B}} = m(x_{L_{1A/B}} - x_s) + y_s \tag{9}$$

Since $x_s = 0$ and $y_s = r_s$, substitution of Eq. (8) into Eq. (9) leads to

$$(1 + m^2)x_{L_{1A/B}}^2 + 2mr_s x_{L_{1A/B}} + (r_s^2 - r_l^2) = 0 \tag{10}$$

Because the preceding equation must be true for either L_{1A} or L_{1B}, there are really two quadratic equations to solve. Only one of these equations is guaranteed to have a real set of solutions. The other may or may not have a solution, depending on whether or not the satellite is above the LTAS. In addition, due to symmetry, the solution to Eq. (10) also has a mirror equivalent on the opposite side of r_s. Thus, the preceding equations have at least two solutions, $(x_{L_{1A}}, y_{L_{1A}})$ and $(x_{L_{2A}}, y_{L_{2A}})$, when the satellite is below the LTAS. At most, there are four solutions, $(x_{L_{1A}}, y_{L_{1A}})$, $(x_{L_{2A}}, y_{L_{2A}})$, $(x_{L_{1B}}, y_{L_{1B}})$, and $(x_{L_{2B}}, y_{L_{2B}})$, if the satellite is above the LTAS. For the intersections located on the $+\hat{x}$ side on Fig. 5, it is clear that $m < 0$. Thus, if $r_s < r_l$, the TL and LTAS intersect when

$$x_{L_{1A}} = \frac{-2mr_s + \sqrt{4m^2 r_s^2 - 4(1 + m^2)(r_s^2 - r_l^2)}}{2(1 + m^2)} \tag{11}$$

Naturally, $x_{L_{1B}}$ does not exist in this case because the satellite is below the UTAS. If, instead, $r_s > r_l$, the TL intersects the LTAS at a second point closer to r_s than that in Eq. (11). The $+\hat{x}$ coordinate of this second intersection is denoted as

$$x_{L_{1B}} = \frac{-2mr_s - \sqrt{4m^2 r_s^2 - 4(1 + m^2)(r_s^2 - r_l^2)}}{2(1 + m^2)} \tag{12}$$

In either case, the equation for the TL leads to

$$y_{L_{1A/B}} = mx_{L_{1A/B}} + r_s \tag{13}$$

and

$$x_{L_{2A/B}} = -x_{L_{1A/B}}; \qquad y_{L_{2A/B}} = y_{L_{1A/B}} \tag{14}$$

C. Intersections of the Tangent Line with the Upper Target Altitude Shell

In the event the RS intersects the UTAS, the coordinates of intersection are easily identified by adapting Eqs. (11–13) to the intersections with the UTAS:

$$x_{U_{1A}} = \frac{1}{2(1 + m^2)}[-2mr_s + \sqrt{4m^2 r_s^2 - 4(1 + m^2)(r_s^2 - r_u^2)}] \tag{15}$$

$$x_{U_{1B}} = \frac{1}{2(1 + m^2)}[-2mr_s - \sqrt{4m^2 r_s^2 - 4(1 + m^2)(r_s^2 - r_u^2)}] \tag{16}$$

$$y_{U_{1A/B}} = mx_{U_{1A/B}} + r_s \tag{17}$$

Once again, symmetry implies that

$$x_{U_{2A/B}} = -x_{U_{1A/B}}; \qquad y_{U_{2A/B}} = y_{U_{1A/B}} \tag{18}$$

D. Intersections of the Tangent Line with the Range Shell

The intersections of the TL with the RS are identified as T_1 and T_2. The Cartesian coordinates of T_1 and T_2 are determined from the following system of equations:

$$x_{T_1}^2 + (y_{T_1} - y_s)^2 = R^2; \qquad y_{T_1} = mx_{T_1} + y_s \tag{19}$$

The solution to this system of equations is determined as

$$x_{T_1} = \frac{R}{\sqrt{1 + m^2}}; \qquad y_{T_1} = mx_{T_1} + r_s \tag{20}$$

for

$$x_{T_2} = -x_{T_1}; \qquad y_{T_2} = y_{T_1} \tag{21}$$

IV. Geometrical Elements of the Coverage Area

As previously mentioned, this study reveals that the coverage area cannot be reduced to a simple generalized equation. Instead, a continuous piecewise differentiable function may be defined to assess the effective coverage area. The primary reason for this complication is that the definition of the coverage area equation changes with the location of the intersection points (T_1, T_2) relative to the intersection points $U_{1A/B}$, $U_{2A/B}$, $L_{1A/B}$, and $L_{2A/B}$. This, in turn, depends on a variety of factors including r_s, R, the size of the LTAS and UTAS, and the size of the THS. To establish a systematic way of identifying the coverage area, the computation is divided into fundamental geometrical elements, mainly triangles, circular segments, and combinations thereof [12]. The effective coverage area is then constructed as the sum of these fundamental area elements. This section summarizes the coverage area of the fundamental shapes employed in constructing the piecewise continuous coverage area function.

A. Triangular Elements

The coverage area function depends strongly on the Cartesian coordinates of each of the fundamental intersections previously defined. Thus, it is convenient to define the area of a triangle as a function of the semiperimeter because this quantity depends only on the lengths of each side of the triangle. The lengths of each side of a triangle are easily identified from Cartesian coordinates using the distance between vertices. The area of a triangle $\mathbf{A}_{\triangle}$, in terms of the semiperimeter, is given by

$$\mathbf{A}_{\triangle}(a,b,c) = \sqrt{s(s-a)(s-b)(s-c)} \tag{22}$$

where a, b, and c denote the lengths of each side and s is the semiperimeter:

$$s = \frac{(a+b+c)}{2} \tag{23}$$

B. Circular Segments

The area of the circular segment $\mathbf{A}_{\Sigma}$ is given by the difference between the area of a circular sector and the area of a triangle, as illustrated in Fig. 6. Subsequently, the equation for the area of the circular segment in Fig. 6 is given by

$$\mathbf{A}_{\Sigma}(r_u, c_{T_3}) = \underbrace{(1/2)\phi r_u^2}_{\text{sector}} - \underbrace{(c_{T_3} r_u)/2\cos(\phi/2)}_{\text{triangle}} \tag{24}$$

In Fig. 6, the angle ϕ is determined as

$$\phi = 2\sin^{-1}[c_{T_3}/(2r_u)] \tag{25}$$

where c_{T_3} denotes the chord of the circular segment and

$$\cos\frac{\phi}{2} = \sqrt{r_u^2 - (c_{T_3}/2)^2}/r_u = \sqrt{4r_u^2 - c_{T_3}^2}/(2r_u) \tag{26}$$

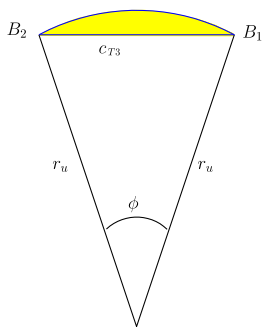

Fig. 6 Area of circular segment.

Substitution of Eqs. (25) and (26) and into Eq. (24) leads to

$$\mathbf{A}_{\Sigma}(r_u, c_{T_3}) = r_u^2\sin^{-1}[c_{T_3}/(2r_u)] - (c_{T_3}/4)\left(\sqrt{4r_u^2 - c_{T_3}^2}\right) \tag{27}$$

C. Composite Teardrop Sectors

A geometrical object derived from the concept of a circular sector is the teardrop sector illustrated in Fig. 7. In this case, the shaded area is denoted by $\mathbf{A}_{\pi_2}$. This type of sector is useful over a certain range of parameters when computing the coverage area, specifically when the range shell is large enough to intersect a target altitude shell on the lowest end of the $-\hat{y}$ side of the plane.

Traditionally, the area of a circular sector is defined as

$$\mathbf{A}_{\pi_1}(R, |\overline{P_1P_2}|) = \tfrac{1}{2}\lambda R^2 \tag{28}$$

where

$$\lambda = \cos^{-1}\left(\frac{|\overline{P_1P_2}|^2 - |\overline{P_1S}|^2 - |\overline{P_2S}|^2}{-2|\overline{P_1S}||\overline{P_2S}|}\right) \tag{29}$$

denotes the angle interior to the sector, $\overline{P_1P_2}$ represents the chord, R is the radius of curvature, and S defines the origin: in this case, the satellite. The area of a teardrop sector can subsequently be expressed as a sum of two fundamental components: a triangle and a circular segment, or its complement. In this case,

$$\mathbf{A}_{\pi_2}(r, R, |\overline{P_1P_2}|) = \begin{cases} \mathbf{A}_{\triangle}(R, |\overline{P_1P_2}|, R) + \mathbf{A}_{\Sigma}(r, |\overline{P_1P_2}|); & R < \sqrt{r_s^2 + r^2} \\ \mathbf{A}_{\triangle}(R, |\overline{P_1P_2}|, R) + \tilde{\mathbf{A}}_{\Sigma}(r, |\overline{P_1P_2}|); & R \geq \sqrt{r_s^2 + r^2} \end{cases} \tag{30}$$

D. Composite Triangular Elements

In the course of devising geometrical arguments to compute the area of coverage, two types of composite triangles are often encountered. In this case, a composite triangle refers to a three-sided geometrical shape for which the sides consist of any combination of line segments and spherical arcs. Figure 8 illustrates one possible type of composite triangle that is sometimes encountered in the process of computing the effective coverage area. In this investigation, this type of composite triangle is denoted Λ_1. This type of geometry is employed in the determination of the coverage area in the examples presented later in this document.

For the geometry in Fig. 8, the radius of $\overset{\frown}{A_2L_{2A}}$ is r_l, and the radius of $\overset{\frown}{A_2T_2}$ is R. The area $\mathbf{A}_{\Lambda_1}$ of this composite triangle is a function of the areas of $\overset{\frown}{A_2L_{2A}}$, $\overset{\frown}{A_2T_2}$, and the triangle defined by vertices A_2, T_2, and L_{2A}. Because the Cartesian coordinates of these vertices are known, we find that

$$\mathbf{A}_{\Sigma}(r_l, |\overline{A_2L_{2A}}|) = r_l^2\sin^{-1}\left(\frac{|\overline{A_2L_{2A}}|}{2r_l}\right) - \frac{|\overline{A_2L_{2A}}|}{4}\left(\sqrt{4r_l^2 - |\overline{A_2L_{2A}}|^2}\right) \tag{31}$$

$$\mathbf{A}_{\Sigma}(R, |\overline{A_2T_2}|) = R^2\sin^{-1}\left(\frac{|\overline{A_2T_2}|}{2R}\right) - \frac{|\overline{A_2T_2}|}{4}\left(\sqrt{4R^2 - |\overline{A_2T_2}|^2}\right) \tag{32}$$

$$\mathbf{A}_{\triangle}(|\overline{A_2T_2}|, |\overline{A_2L_{2A}}|, |\overline{T_2L_{2A}}|) = \sqrt{s(s - |\overline{A_2T_2}|)(s - |\overline{A_2L_{2A}}|)(s - |\overline{T_2L_{2A}}|)} \tag{33}$$

Thus, the equation that describes the area of the composite triangle in Fig. 8 is given by

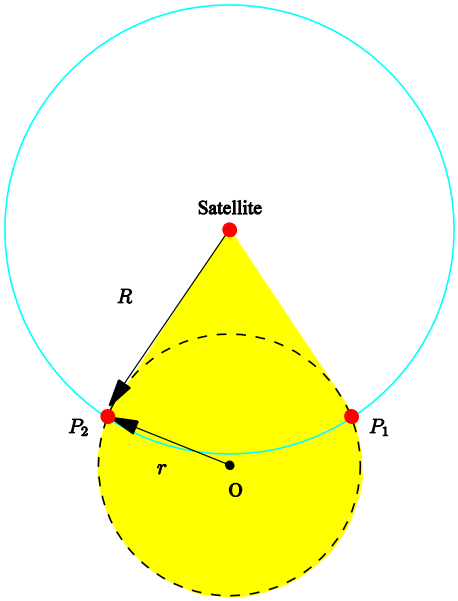

Fig. 7 Area of a teardrop pattern.

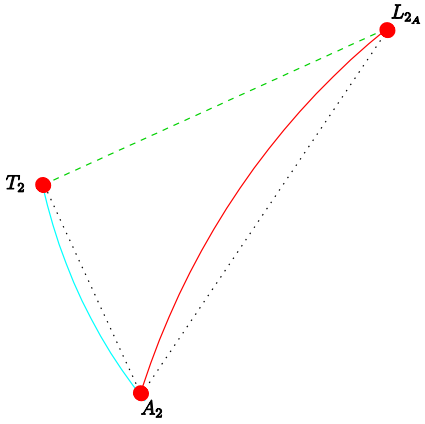

Fig. 8 Composite triangle Λ_1.

$$\mathbf{A}_{\Lambda_1}(r_l, R, |\overline{A_2T_2}|, |\overline{A_2L_{2A}}|, |\overline{T_2L_{2A}}|) = \mathbf{A}_{\triangle}(|\overline{A_2T_2}|, |\overline{A_2L_{2A}}|, |\overline{T_2L_{2A}}|) - \mathbf{A}_{\Sigma}(r_l, |\overline{A_2L_{2A}}|) + \mathbf{A}_{\Sigma}(R, |\overline{A_2T_2}|) \quad (34)$$

where

$$s = \tfrac{1}{2}(|\overline{A_2T_2}| + |\overline{A_2L_{2A}}| + |\overline{T_2L_{2A}}|) \quad (35)$$

and

$$|\overline{A_2T_2}| = \sqrt{(x_{A_2} - x_{T_2})^2 + (y_{A_2} - y_{T_2})^2} \quad (36)$$

$$|\overline{A_2L_{2A}}| = \sqrt{(x_{A_2} - x_{L_{2A}})^2 + (y_{A_2} - y_{L_{2A}})^2} \quad (37)$$

$$|\overline{T_2L_{2A}}| = \sqrt{(x_{T_2} - x_{L_{2A}})^2 + (y_{T_2} - y_{L_{2A}})^2} \quad (38)$$

Another type of composite triangle Λ_2 is illustrated in Fig. 9. This type of geometry is typically visible when the satellite crosses one of the target altitude shells, in this case the UTAS. The area of the geometry illustrated in Fig. 9 is determined as

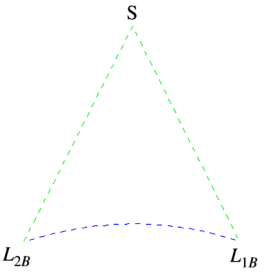

Fig. 9 Composite triangle Λ_2.

$$\mathbf{A}_{\Lambda_2}(r_l, |\overline{L_{2B}S}|, |\overline{L_{1B}L_{2B}}|, |\overline{L_{1B}S}|) = \mathbf{A}_{\triangle}(|\overline{L_{2B}S}|, |\overline{L_{1B}L_{2B}}|, |\overline{L_{1B}S}|) - \mathbf{A}_{\Sigma}(r_l, |\overline{L_{1B}L_{2B}}|) \quad (39)$$

E. Intersection of Circular Elements

The shaded area in Fig. 10 is denoted as $\mathbf{A}_{\mathrm{RS}\cap\mathrm{LTAS}}$. However, the formulation presented here is also applicable to $\mathbf{A}_{\mathrm{RS}\cap\mathrm{UTAS}}$. Let O denote the origin in Fig. 10 such that $|\overline{OA_1}| = r_l$ and $|\overline{SA_1}| = R$. The shaded area in Fig. 10 is easily determined by adding the area of two adjacent circular segments, each individually determined from Eq. (27):

$$\mathbf{A}_{\mathrm{RS}\cap\mathrm{LTAS}}(r_l, R, |\overline{A_1A_2}|) = \mathbf{A}_{\Sigma}(r_l, |\overline{A_1A_2}|) + \mathbf{A}_{\Sigma}(R, |\overline{A_1A_2}|) \quad (40)$$

This equation, however, is not applicable for all possible types of intersections between the two circles. The actual value of the coverage area depends on where the two circles intersect and the location of these points relative to S and O. Figure 11 illustrates four possible cases relevant to this investigation that must be considered in accurately computing the area of intersection. More specifically, Figs. 11a and 11b are associated with $R < r_l$, whereas Figs. 11c and 11d correspond to $R \geq r_l$. Figure 11a is further associated with $r_s > \sqrt{r_l^2 - R^2}$, whereas Fig. 11b is associated with $r_s \leq \sqrt{r_l^2 - R^2}$. Similarly, Fig. 11c corresponds to $r_s > \sqrt{R^2 - r_l^2}$, whereas Fig. 11d implies $r_s \leq \sqrt{R^2 - r_l^2}$. The area of intersection between the RS and the LTAS is subsequently determined as

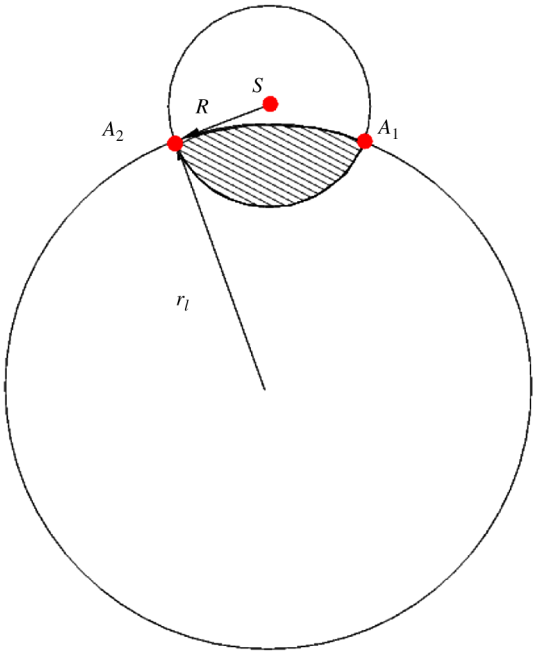

Fig. 10 Area of intersection between two circles.

$$\mathbf{A}_{\mathrm{RS}\cap\mathrm{LTAS}} = \begin{cases} \mathbf{A}_\Sigma(R, |\overline{A_1A_2}|) + \mathbf{A}_\Sigma(r_l, |\overline{A_1A_2}|); & \begin{cases} r_l > R \quad \text{and} \quad r_s > \sqrt{r_l^2 - R^2} \\ \text{or} \\ r_l \le R \quad \text{and} \quad r_s > \sqrt{R^2 - r_l^2} \end{cases} \\ \pi R^2 - \mathbf{A}_\Sigma(R, |\overline{A_1A_2}|) + \mathbf{A}_\Sigma(r_l, |\overline{A_1A_2}|); & \{r_l > R \quad \text{and} \quad r_s \le \sqrt{r_l^2 - R^2} \\ \pi r_l^2 - \mathbf{A}_\Sigma(r_l, |\overline{A_1A_2}|) + \mathbf{A}_\Sigma(R, |\overline{A_1A_2}|); & \{r_l \le R \quad \text{and} \quad r_s \le \sqrt{R^2 - r_l^2} \end{cases} \tag{41}$$

The three cases listed in Eq. (41), in the order presented, are associated with Figs. 11a, 11d, 11b, and 11c, respectively.

V. Single Satellite Above the Horizon Coverage Area

The area calculation is divided into three main cases. Case 1 corresponds to a satellite located below the LTAS and above the THS, $r_t \le r_s < r_l$. In Case 2, the satellite orbit exists between the LTAS and UTAS, $r_l \le r_s < r_u$. Finally, a satellite situated above the UTAS leads to case 3, $r_s \ge r_u$. Within each of these cases, the specific combination of geometrical components selected for the computation of the coverage area is further influenced by the size of the range shell R. The magnitude of R, given a specified value of r_s, subsequently affects the intersections of the range shell along the tangent line (T_1 and T_2). Because there are two such intersections, symmetric about the $\hat{y}$ axis, the following discussion focuses strictly on the intersection that defines the line segment $|\overline{T_2S}|$. The notation adopted in this document to refer to these individual cases is summarized in Tables 1–3.

The illustrations in Figs. 12–14 offer graphical examples of each of these subcases so that the reader can better visualize why the area calculation is affected. The definitions in Tables 1–3 are subsequently employed to identify the corresponding coverage area equations listed in Tables 4–6. Note that there are a total of 18 cases to consider in computing the coverage area, not including specific subcases introduced by Eq. (41). In Tables 1–3, the symbol Ø implies an empty set. Thus, $|\overline{A_1A_2}| = \text{Ø}$ indicates the RS does not intersect the LTAS.

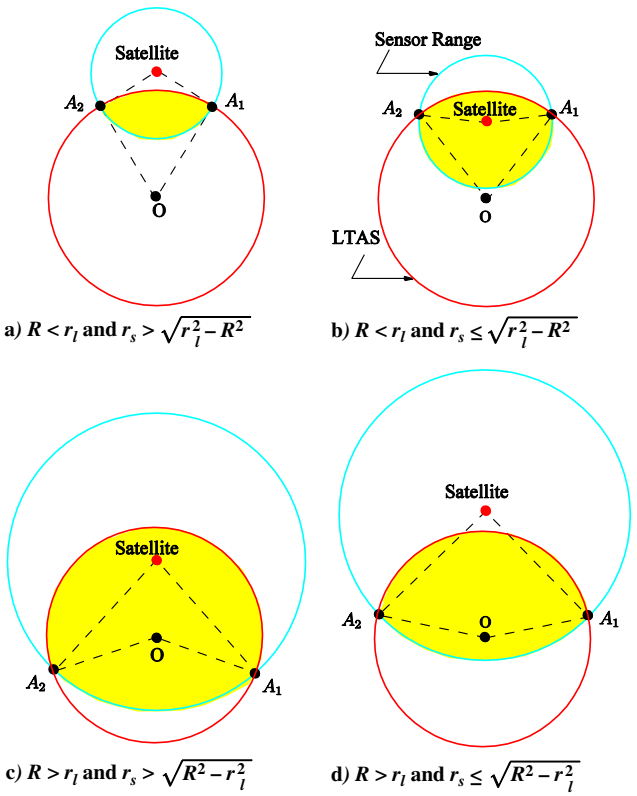

Fig. 11 Area of intersection between RS and LTAS.

Naturally, there is no unique way of representing the coverage area for a specific set of parameters. In fact, two individuals attempting to compute the same coverage area might choose to decompose the same region into a completely different set of geometrical elements. Thus, the cases summarized in Tables 4–6 are merely one possible representation of the area equation for each case. Care is exercised, however, in selecting a formulation that simplifies the calculation and leads to a systematic approach for constructing the resulting continuous piecewise differentiable function that describes the coverage area.

Ultimately, the contents of Tables 4–6 define an objective function that can be subsequently implemented in an optimization process to identify the optimal altitude that maximizes the constrained ATH coverage area. An example of this process is presented next. To demonstrate how one arrives at each of the equations in Tables 4–6, consider case 2(d.i). The coverage area equation for case 2(d.i) can be decomposed into several area elements, including $\mathbf{A}_{\mathrm{UTAS}\cap\mathrm{RS}}$, $\mathbf{A}_{\mathrm{LTAS}\cap\mathrm{RS}}$, $\mathbf{A}_{\Lambda_2}$, and $\mathbf{A}_{\Lambda_1}$. Figure 15 illustrates how the total coverage area is constructed from these elements.

A. Example 1

Figure 16a depicts the coverage area as a function of satellite altitude for a fixed sensor range. As expected, the coverage area is

Table 1 Coverage area subcases for $r_t \le r_s < r_l$ (see Fig. 12)

Condition	Case no.
$\lvert\overline{T_2S}\rvert < \lvert\overline{L_{2A}S}\rvert$	1(a)
$\lvert\overline{L_{2A}S}\rvert \le \lvert\overline{T_2S}\rvert < \lvert\overline{U_{2A}S}$	1(b.i): $\lvert\overline{A_1A_2}\rvert \ne \text{Ø}$
	1(b.ii): $\lvert\overline{A_1A_2}\rvert = \text{Ø}$
$\lvert\overline{U_{2A}S}\rvert \le \lvert\overline{T_2S}\rvert$	1(c.i): $\lvert\overline{A_1A_2}\rvert \ne \text{Ø}$
	1(c.ii): $\lvert\overline{A_1A_2}\rvert = \text{Ø}$

Table 2 Coverage area subcases for $r_l \le r_s < r_u$ (see Fig. 13)

Condition	Case no.
$\lvert\overline{T_2S}\rvert < \lvert\overline{L_{2B}S}\rvert$	2(a)
$\lvert\overline{L_{2B}S}\rvert \le \lvert\overline{T_2S}\rvert < \lvert\overline{L_{2A}S}\rvert$	2(b)
$\lvert\overline{L_{2A}S}\rvert \le \lvert\overline{T_2S}\rvert < \lvert\overline{U_{2A}S}\rvert$	2(c.i): $\lvert\overline{A_1A_2}\rvert \ne \text{Ø}$
	2(c.ii) $\lvert\overline{A_1A_2}\rvert = \text{Ø}$
$\lvert\overline{U_{2A}S}\rvert \le \lvert\overline{T_2S}\rvert$	2(d.i): $\lvert\overline{A_1A_2}\rvert \ne \text{Ø}$
	2(d.ii): $\lvert\overline{A_1A_2}\rvert = \text{Ø}$

Table 3 Coverage area subcases for $r_u \le r_s < r_{s_3}$ (see Fig. 14)

Condition no.	Case no.
$\lvert\overline{T_2S}\rvert < \lvert\overline{U_{2B}S}\rvert$	3(a)
$\lvert\overline{U_{2B}S}\rvert \le \lvert\overline{T_2S}\rvert < \lvert\overline{L_{2B}S}\rvert$	3(b)
$\lvert\overline{L_{2B}S}\rvert \le \lvert\overline{T_2S}\rvert < \lvert\overline{L_{2A}S}\rvert$	3(c)
$\lvert\overline{L_{2A}S}\rvert \le \lvert\overline{T_2S}\rvert < \lvert\overline{U_{2A}S}\rvert$	3(d.i): $\lvert\overline{A_1A_2}\rvert \ne \text{Ø}$
	3(d.ii): $\lvert\overline{A_1A_2}\rvert = \text{Ø}$
$\lvert\overline{U_{2A}S}\rvert \le \lvert\overline{T_2S}\rvert$	3(e.i): $\lvert\overline{A_1A_2}\rvert \ne \text{Ø}$
	3(e.ii): $\lvert\overline{A_1A_2}\rvert = \text{Ø}$

Table 4 Coverage area for $r_t \le r_s < r_l$ (see Fig. 12)

Case no.	Area
1(a)	$\mathbf{A} = \mathbf{A}_{\text{UTAS}\cap\text{RS}} - \mathbf{A}_{\text{LTAS}\cap\text{RS}}$
1(b.i)	$\mathbf{A} = \mathbf{A}_{\text{UTAS}\cap\text{RS}} - \mathbf{A}_{\text{LTAS}\cap\text{RS}} - 2\mathbf{A}_{\Lambda_1}(R, r_l, \lvert\overline{T_2L_{2A}}\rvert, \lvert\overline{T_2A_2}\rvert, \lvert\overline{A_2L_{2A}}\rvert)$
1(b.ii)	$\mathbf{A} = \mathbf{A}_{\text{UTAS}\cap\text{RS}} - \pi r_l^2 - \mathbf{A}_{\pi_1}(R, \lvert\overline{T_1T_2}\rvert) + \mathbf{A}_{\pi_2}(r_l, R, \lvert\overline{L_{1A}L_{2A}}\rvert)$
1(c.i)	$\mathbf{A} = \mathbf{A}_{\text{UTAS}\cap\text{RS}} - \mathbf{A}_{\text{LTAS}\cap\text{RS}} - 2\mathbf{A}_{\Lambda_1}(r_l, R, \lvert\overline{T_2L_{2A}}\rvert, \lvert\overline{T_2A_2}\rvert, \lvert\overline{A_2L_{2A}}\rvert) + 2\mathbf{A}_{\Lambda_1}(r_u, R, \lvert\overline{T_2U_{2A}}\rvert, \lvert\overline{T_2B_2}\rvert, \lvert\overline{B_2U_{2A}}\rvert)$
1(c.ii)	$\mathbf{A} = \pi r_u^2 - \pi r_l^2 - \mathbf{A}_{\pi_2}(r_u, R, \lvert\overline{U_{1A}U_{2A}}\rvert) + \mathbf{A}_{\pi_2}(r_l, R, \lvert\overline{L_{1A}L_{2A}}\rvert)$

Table 5 Coverage area for $r_l \le r_s < r_u$ (see Fig. 13)

Case no.	Area
2(a)	$\mathbf{A} = \mathbf{A}_{\text{UTAS}\cap\text{RS}} - \mathbf{A}_{\pi_1}(R, \lvert\overline{T_1T_2}\rvert)$
2(b)	$\mathbf{A} = \mathbf{A}_{\text{UTAS}\cap\text{RS}} - \mathbf{A}_{\text{LTAS}\cap\text{RS}} - \mathbf{A}_{\Lambda_2}(r_l, \lvert\overline{L_{1B}S}\rvert, \lvert\overline{L_{1B}L_{2B}}\rvert, \lvert\overline{L_{2B}S}\rvert)$
2(c.i)	$\mathbf{A} = \mathbf{A}_{\text{UTAS}\cap\text{RS}} - \mathbf{A}_{\text{LTAS}\cap\text{RS}} - \mathbf{A}_{\Lambda_2}(r_l, \lvert\overline{L_{1B}S}\rvert, \lvert\overline{L_{1B}L_{2B}}\rvert, \lvert\overline{L_{2B}S}\rvert) - 2\mathbf{A}_{\Lambda_1}(r_l, R, \lvert\overline{T_2L_{2A}}\rvert, \lvert\overline{T_2A_2}\rvert, \lvert\overline{A_2L_{2A}}\rvert)$
2(c.ii)	$\mathbf{A} = \mathbf{A}_{\text{UTAS}\cap\text{RS}} - \mathbf{A}_{\text{LTAS}\cap\text{RS}} - \mathbf{A}_{\Lambda_2}(r_l, \lvert\overline{L_{1B}S}\rvert, \lvert\overline{L_{1B}L_{2B}}\rvert, \lvert\overline{L_{2B}S}\rvert) - \mathbf{A}_{\pi_1}(R, \lvert\overline{T_1T_2}\rvert) + \mathbf{A}_{\pi_2}(r_l, R, \lvert\overline{L_{1A}L_{2A}}\rvert)$
2(d.i)	$\mathbf{A} = \mathbf{A}_{\text{UTAS}\cap\text{RS}} - \mathbf{A}_{\text{LTAS}\cap\text{RS}} - \mathbf{A}_{\Lambda_2}(r_l, \lvert\overline{L_{1B}S}\rvert, \lvert\overline{L_{1B}L_{2B}}\rvert, \lvert\overline{L_{2B}S}\rvert) - \mathbf{2A}_{\Lambda_1}(r_l, R, \lvert\overline{T_2L_{2A}}\rvert, \lvert\overline{T_2A_2}\rvert, \lvert\overline{A_2L_{2A}}\rvert)$ $\mathbf{A} = \mathbf{A} + \mathbf{2A}_{\Lambda_1}(r_u, R, \lvert\overline{T_2U_{2A}}\rvert, \lvert\overline{T_2B_2}, \rvert, \lvert\overline{B_2U_{2A}}\rvert)$
2(d.ii)	$\mathbf{A} = \pi r_u^2 - \pi r_l^2 - \mathbf{A}_{\pi_2}(r_u, R, \lvert\overline{U_{1A}U_{2A}}\rvert) + \mathbf{A}_{\pi_2}(r_l, R, \lvert\overline{L_{1A}L_{2A}}\rvert) - \mathbf{A}_{\Lambda_2}(r_1, \lvert\overline{L_{1B}S}\rvert, \lvert\overline{L_{1B}L_{2B}}\rvert\rvert\overline{L_{2B}S}\rvert)$

Table 6 Coverage area for $r_l \le r_s < r_u$ (see Fig. 14)

Case no.	Area
3(a)	$\mathbf{A} = \mathbf{0}$
3(b)	$\mathbf{A} = \mathbf{A}_{\text{UTAS}\cap\text{RS}} - \mathbf{A}_{\pi_1}(R, \lvert\overline{T_1T_2}\rvert) + \mathbf{A}_{\Lambda_2}(r_u, \lvert\overline{U_{2B}S}\rvert, \lvert\overline{U_{1B}U_{2B}}\rvert, \lvert\overline{U_{1B}S}\rvert)$
3(c)	$\mathbf{A} = \mathbf{A}_{\text{UTAS}\cap\text{RS}} - \mathbf{A}_{\Lambda_2}(r_l, \lvert\overline{L_{1B}S}\rvert, \lvert\overline{L_{1B}L_{2B}}\rvert, \lvert\overline{L_{2B}S}\rvert) + \mathbf{A}_{\Lambda_2}(r_u, \lvert\overline{U_{1B}S}\rvert, \lvert\overline{U_{1B}U_{2B}}\rvert, \lvert\overline{U_{2B}S}\rvert)$
3(d.i)	$\mathbf{A} = \mathbf{A}_{\text{UTAS}\cap\text{RS}} - \mathbf{A}_{\Lambda_2}(r_l, \lvert\overline{L_{1B}S}\rvert, \lvert\overline{L_{1B}L_{2B}}\rvert, \lvert\overline{L_{2B}S}\rvert) + \mathbf{A}_{\Lambda_2}(r_u, \lvert\overline{U_{1B}S}\rvert, \lvert\overline{U_{1B}U_{2B}}\rvert, \lvert\overline{U_{2B}S}\rvert)$ $\mathbf{A} = \mathbf{A} - \mathbf{2A}_{\Lambda_1}(r_l, R, \lvert\overline{T_2L_{2A}}\rvert, \lvert\overline{T_2A_2}\rvert, \lvert\overline{A_2L_{2A}}\rvert)$
3(d.ii)	$\mathbf{A} = \mathbf{A}_{\text{UTAS}\cap\text{RS}} - \pi r_l^2 - \mathbf{A}_{\Lambda_2}(r_l, \lvert\overline{L_{1B}S}\rvert, \lvert\overline{L_{1B}L_{2B}}\rvert, \lvert\overline{L_{2B}S}\rvert) + \mathbf{A}_{\Lambda_2}(r_u, \lvert\overline{U_{1B}S}\rvert, \lvert\overline{U_{1B}U_{2B}}\rvert, \lvert\overline{U_{2B}S}\rvert)$ $\mathbf{A} = \mathbf{A} - \mathbf{A}_{\pi_2}(R, \lvert\overline{T_1T_2}\rvert) + \mathbf{A}_{\pi_2}(r_l, R, \lvert\overline{L_{1A}L_{2A}}\rvert)$
3(e.i)	$\mathbf{A} = \mathbf{A}_{\text{UTAS}\cap\text{RS}} - \mathbf{A}_{\text{LTAS}\cap\text{RS}} - \mathbf{A}_{\Lambda_2}(r_l, \lvert\overline{L_{1B}S}\rvert, \lvert\overline{L_{1B}L_{2B}}\rvert, \lvert\overline{L_{2B}S}\rvert) + \mathbf{A}_{\Lambda_2}(r_u, \lvert\overline{U_{1B}S}\rvert, \lvert\overline{U_{1B}U_{2B}}\rvert, \lvert\overline{U_{2B}S}\rvert)$ $\mathbf{A} = \mathbf{A} - \mathbf{2A}_{\Lambda_1}(r_l, R, \lvert\overline{T_2L_{2A}}\rvert, \lvert\overline{T_2A_2}\rvert, \lvert\overline{A_2L_{2A}}\rvert) + \mathbf{2A}_{\Lambda_1}(r_u, R, \lvert\overline{T_2U_{2A}}\rvert, \lvert\overline{T_2B_2}\rvert, \lvert\overline{B_2U_{2A}}\rvert)$
3(e.ii)	$\mathbf{A} = \pi r_u^2 - \pi r_l^2 - \mathbf{A}_{\pi_2}(r_u, R, \lvert\overline{U_{1A}U_{2A}}\rvert) + \mathbf{A}_{\pi_2}(r_1, R, \lvert\overline{L_{1A}L_{2A}}\rvert) - \mathbf{A}_{\Lambda_2}(r_l, \lvert\overline{L_{1B}S}\rvert, \lvert\overline{L_{1B}L_{2B}}\rvert, \lvert\overline{L_{2B}S}\rvert)$ $\mathbf{A} = \mathbf{A} + \mathbf{A}_{\Lambda_2}(r_u, \lvert\overline{U_{1B}S}\rvert, \lvert\overline{U_{1B}U_{2B}}\rvert, \lvert\overline{U_{2B}S}\rvert)$

nullified as $r \to r_{s_3}$. In this particular example, the maximum coverage area is achieved when the satellite altitude is 1353 km for $R = 5000$, $h_l = 1000$, $h_u = 5000$, and $h_t = 100$ km. The corresponding geometrical configuration is illustrated in Fig. 16b. It is interesting to note that, unlike the BTH case, maximizing θ does not lead to maximum coverage area. Also, unlike the traditional ATH case, $R_1 + R_2$ does not offer the maximum coverage area for a fixed altitude band. In fact, the results of this study indicate that there is no obvious relation between the coverage angle and the maximum coverage area. Thus, the methodology presented here is an important step toward identifying optimal constellations for maximum ATH altitude band limited coverage.

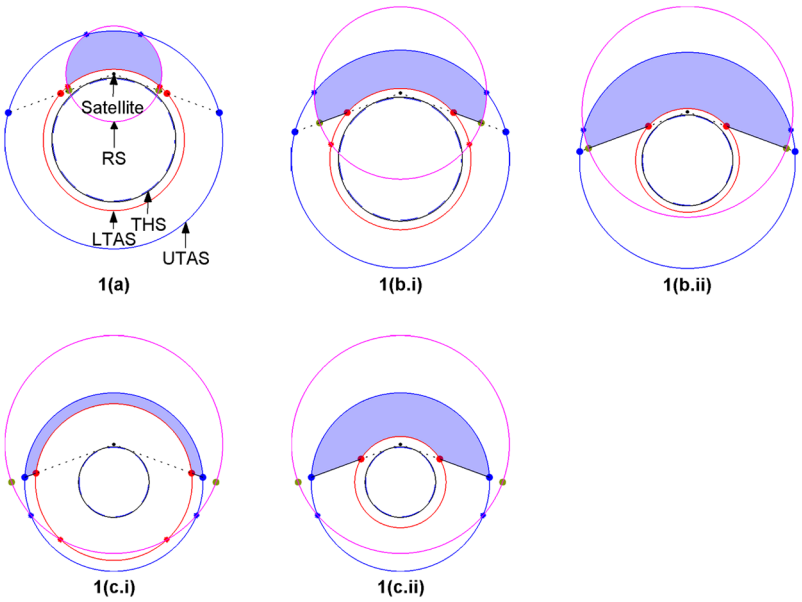

Fig. 12 Case 1 scenarios.

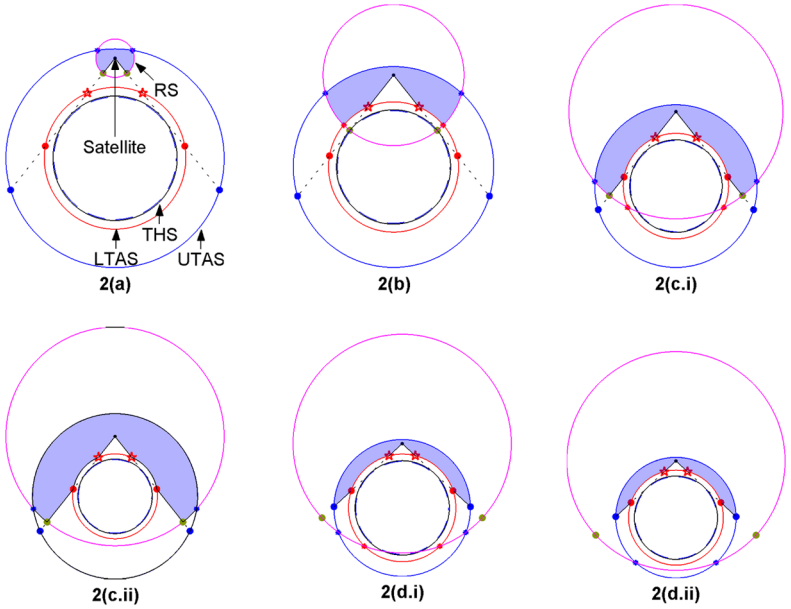

Fig. 13 Case 2 scenarios.

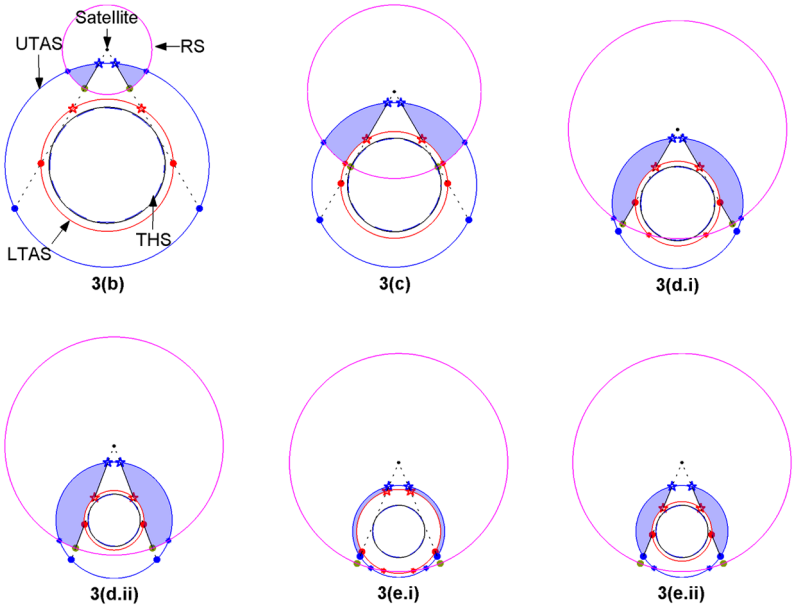

Fig. 14 Case 3 scenarios.

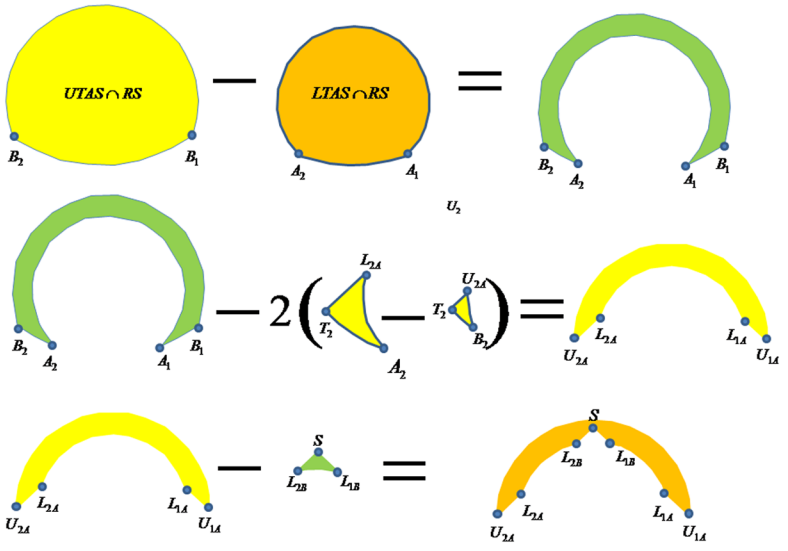

Fig. 15 Coverage area calculation for case 2(d.i).

B. Example 2

A more complete analysis of the optimal solution space is presented in Figs. 17a and 17b. These figures depict contours of optimal satellite altitude as a function of sensor range and upper target altitude. In this particular example, the tangent height is defined as 100 km and the lower target altitude is fixed at 600 km to simplify the visualization of the optimal altitude trends. For completeness, the satellite altitudes considered range from 100 to 15,000 km. The UTAS altitude values employed in this example span from 700 to 10,000 km. Finally, the sensor range is sampled between 10 and 20,000 km. These three parameter spaces are used to define a three-dimensional $5000 \times 5000 \times 5000$ parameter grid, subsequently used to identify the optimal satellite altitude for each combination of r_u and R. That is, for each combination of r_u and R, the coverage area is evaluated 5000 times for a satellite altitude between 100 and 15,000 km. From those results, a maximum coverage area is tentatively selected based on programming logic. Once a candidate maximum is identified, a one-dimensional line search is performed to obtain a more accurate estimate of the optimal satellite altitude.

The most interesting features of Fig. 17b are the two ridge lines that separate the central region of the contours from the exterior regions. Numerical examination of these ridge lines reveals that the lower ridge line corresponds to the set of optimal solutions associated with a critical intersection between L_{2A}, T_2, and A_2. By symmetry, at that same altitude, there is also an intersection between L_{1A}, T_1, and A_1. Similarly, the upper ridge line is representative of optimal solutions associated with the critical intersection of U_{2A}, T_2, and B_2.

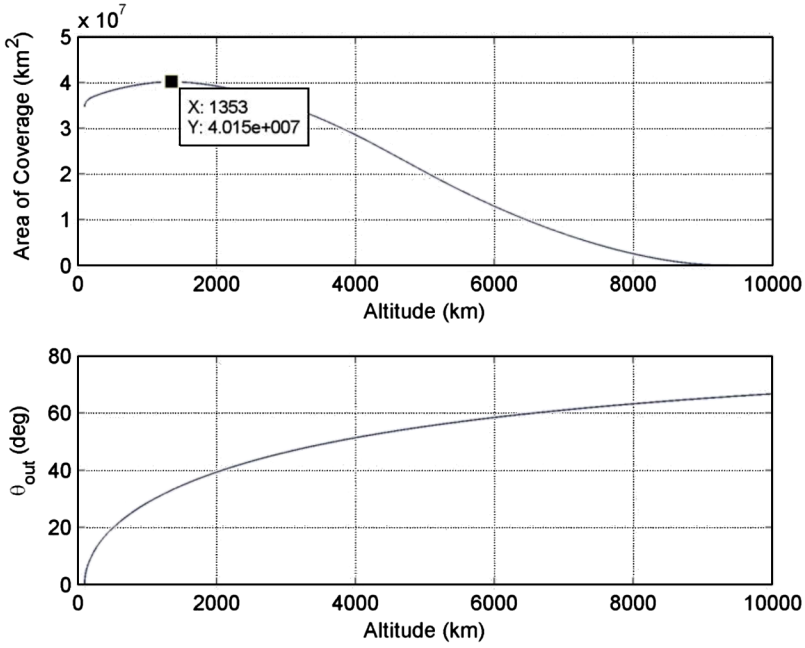

a) Area of coverage (top) and exit angle θ_{out} (bottom) vs. altitude for example 1

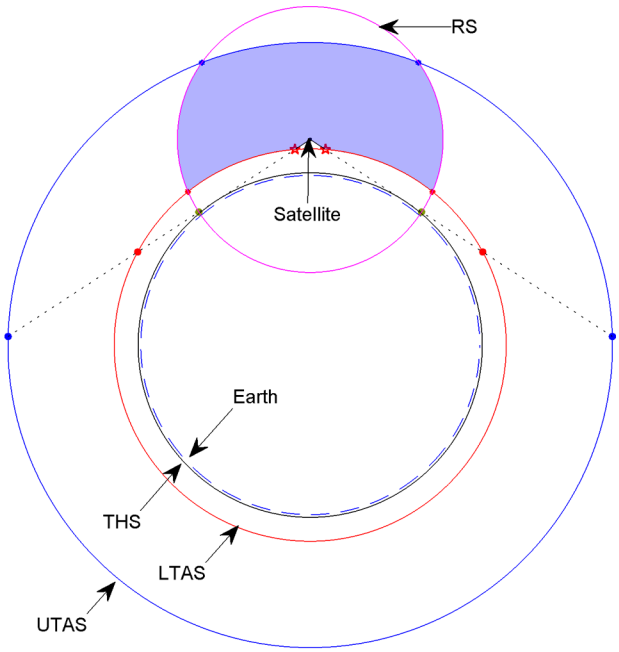

b) Optimal Satellite Position and Resulting Coverage Area for Example 1

Fig. 16 Example 1: a) coverage area and θ_{out} vs h_s, and b) resulting optimal configuration.

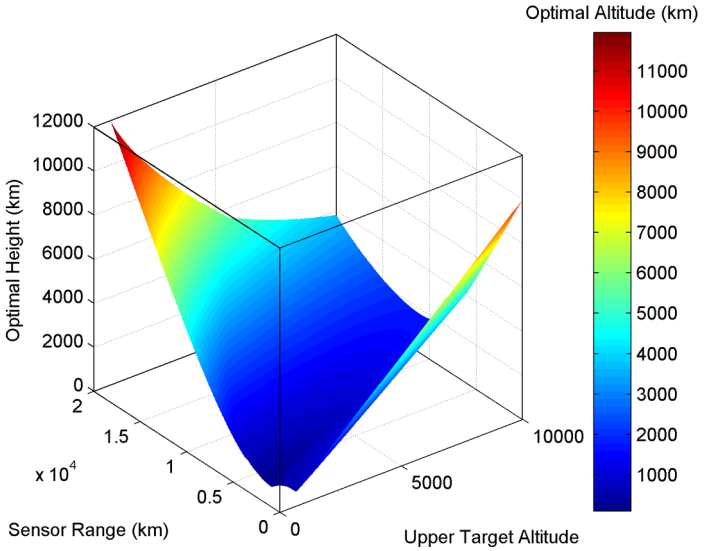

a)

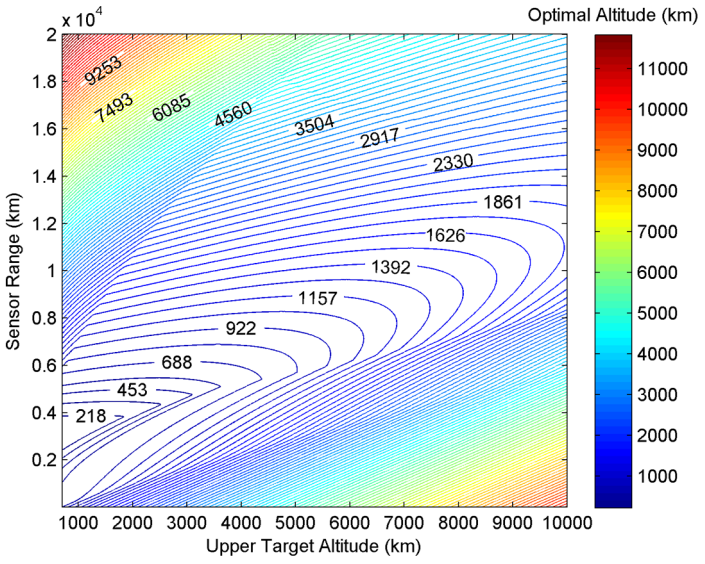

b)

Fig. 17 Sample a) optimal height surface, and b) contours.

It is also interesting to note that, in the exterior regions outlined by these ridge lines, the relation between the maximum coverage area and the sensor and upper target altitudes seems relatively linear, unlike that observed in the interior region. Although the significance of this trend is of interest for future investigations, it is not the focus of the present study. Every design problem is linked to a different set of constraints and parameters, all of which affect the trends outlined in these figures. Thus, it would be premature to draw any globally definitive conclusions from these results. However, the results presented here do offer a proof of concept for the proposed methodology. The algorithm and graphical tools developed during the course of this study are an important first step toward the identification of optimal constellations for maximum dual-altitude band ATH coverage. In that case, the goal is to identify the minimum number of satellites and the optimal arrangement required to maximize ATH coverage over a prespecified altitude and latitude band.

VI. Conclusions

The present study focuses on the identification of the optimal satellite altitude necessary to achieve maximum coverage of targets against a space background within a prespecified dual-altitude band assuming an omnidirectional sensor range. Unlike earlier results regarding optimal BTH coverage and single-altitude band ATH coverage, no direct correlation exists between the coverage angle and the maximum coverage area. This investigation further reveals that no simple closed-form equation exists when defining the ATH coverage area between a prespecified dual-altitude band. However, the coverage area, in this case, can be represented as a nonlinear continuous piecewise differentiable function. The key to computing the coverage area in this more complex case lies in the proper identification of the mutual intersections between the TL cone, the RS, the UTAS, and the LTAS. All relevant geometrical arrangements are identified and discussed in this study. The most important outcome of this study is the successful identification of a continuous piecewise differentiable objective function that relates the dual-altitude band ATH coverage area (i.e., the area of the cross section of axially symmetric coverage volume) to the satellite altitude, sensor range, and the dimensions of the LTAS, UTAS, and THS. This represents a fundamental first step toward a systematic approach for the design of optimal constellations for maximum dual-altitude band ATH coverage, specifically, constellations that may potentially impose additional constraints on the visible region of interest, such as a prespecified latitude band.

Acknowledgments

This work was performed at The Aerospace Corporation and at the University of Texas at Austin. The authors would like to thank Bill Adams and Tom Lang of The Aerospace Corporation for their valuable input during the course of this investigation.

References

[1] Wertz, J. R., *Mission Geometry; Orbit and Constellation Design and Management-Spacecraft Orbit and Attitude Systems*, 1st ed., Microcosm Press, El Segundo, CA, and Kluwer Academic, Norwell, MA, 2001.

[2] Walker, J. G., "Circular Orbit Patterns Providing Continuous Whole Earth Coverage," Royal Aircraft Establishment, TR 70211, Nov. 1970.

[3] Walker, J. G., "Continuous Whole-Earth Coverage by Circular-Orbit Satellite Patterns," Royal Aircraft Establishment, TR 77044, March 1977.

[4] Walker, J. G., "Satellite Constellations," *Journal of the British Interplanetary Society*, Vol. 37, Dec. 1984, pp. 559–572.

[5] Adams, W. S., and Rider, L., "Circular Polar Constellations Providing Continuous Single or Multiple Coverage Above a Specified Latitude," *Journal of the Astronautical Sciences*, Vol. 35, No. 2, April–June 1987, pp. 155–192.

[6] Lang, T. J., "Optimal Low Earth Orbit Constellations for Continuous Global Coverage," *Proceedings of the AAS/AIAA Astrodynamics Conference*, Univelt, San Diego, CA, 1994, pp. 1199–1216.

[7] Gordon, K. J., "The Computation of Satellite Constellation Range Characteristics," AIAA Paper 94-3704, Aug. 1994.

[8] Beste, D. C., "Design of Satellite Constellations for Optimal Continuous Coverage," *IEEE Transactions on Aerospace and Electronic Systems*, Vol. AES-14, Inst. of Electrical and Electronics Engineers, New York, May 1978, pp. 466–473.

[9] Rider, L., "Optimal Orbital Constellations for Global Viewing of Targets Against a Space Background," *Optical Engineering*, Vol. 19, No. 2, March–April 1980, pp. 219–223.

[10] Rider, L., "Design of Low to Medium Altitude Surveillance Systems Providing Continuous Multiple Above-the-Horizon Viewing," *Optical Engineering*, Vol. 28, No. 1, Jan. 1989, pp. 25–29.

[11] Hanson, J. M., and Linden, A. N., "Improved Low-Altitude Constellation Design Methods," *Journal of Guidance, Control, and Dynamics*, Vol. 12, No. 2, March–April 1989, pp. 228–236. doi:10.2514/3.20395

[12] Fewell, M. P., "Area of Common Overlap of Three Circles," Maritime Operations Div., Defense Science and Technology Organization TN DSTO-TN-0722.

C. Kluever
Associate Editor